Electron Microscopy and Magnetic Properties of Tetra(n-butyl) ammonium salts of $[Ni(dmbit)_2]^{1-}$ and $[Ni(dmbbip)_2]^{1-}$ ($dmbit^{2-}$: $C_7H_2S_5$: 2-thiobenzo[*d*]-1,3-dithiole-5,6-dithiolate; $dmbbip^{2-}$: $C_{12}H_{16}S_4$: 1,2-bis(isopropylthio)benzene-4,5-dithiolate)

Dong-Youn Noh*, Mi-Jeong Kang, Ha-Jin Lee, Jong-Hyun Kim, and Jin-Ho Choy†

Department of Chemistry, Seoul Woman's University, Seoul 139-774, Korea
†Department of Chemistry, Seoul National University, Seoul 151-742, Korea
Received September 22, 1995

Monoanionic nickel(III) complexes, $[Ni(dmbit)_2]^{1-}$ and $[Ni(dmbbip)_2]^{1-}$ where $dmbit^{2-}$ and $dmbbip^{2-}$ denote 2-thiobenzo[*d*]-1,3-dithiole-5,6-dithiolate and 1,2-bis(isopropylthio)benzen-4,5-dithiolate, respectively, have been synthesized by the iodine oxidation of dianionic complexes. In the scanning electron microscopic (SEM) images, these complexes show the well-grown two-dimensional layered structures which are clearly comparable to the dianionic ones with three-dimensional structures. Magnetic susceptibilities of nickel(III) complexes are fitted well with the two-dimensional Heisenberg antiferromagnet model of S=1/2 system resulting in the spin-exchange parameters ($|J|/k$) of 11.4 K and 0.45 K, respectively. The weaker magnetic interaction in $[Ni(dmbbip)_2]^{1-}$ is resulted from the bulky isopropyl groups on the periphery of dmbbip ligand. EPR measurements for $[Ni(dmbit)_2]^{1-}$ give the signal with axial symmetry and the anisotropic g-values for low-spin nickel(III) ($g_{//}=2.158$, $g_{\perp}=2.030$, $g_{av}=2.074$ at 300 K; $g_{//}=2.162$, $g_{\perp}=2.038$, $g_{av}=2.080$ at 77 K). It is therefore concluded that nickel(II) is oxidized to nickel(III), rather than $dmbit^{2-}$ and $dmbbip^{2-}$ ligands are, by the iodine oxidation. The paramagnetic Ni(III) would be located in the axial symmetry(D_{4h}) with the electronic configuration of $(d_{xz}^2 d_{yz}^2 d_{z^2}^2 d_{xy}^1 d_{x^2-y^2}^0)$.

Introduction

Since the discovery of superconductivity in $(TTF)[M(dmit)_2]_2$ (M=Ni[1], Pd[2]; TTF=tetrathiafulvalene), many efforts have been focused on the developement of new metal-coordinated organic conductors and superconductors.[3~5] Some more superconductors with dmit-ligand have been reported thereafter.[6] But many other complexes were found to be semiconductors or insulators such as $[M(dddt)_2]^{x-}$ (M=Ni, Au; dddt=5,6-dihydro-1,4-dithiin-2,3-dithiolate),[7~8] $[Ni(ddt)_2]^{1-}$ (ddt=1,4-dithiin-2,3-dithiolate)[9] and $[Ni(pddt)_2]^{1-}$ (pddt=1,3-propane-diyldithioethylene-1,2-dithiolate).[10] Dmbit and dmbbip ligands belong to this category, the former of which was prepared by modifying dmit-ligand to extend π-conjugation system on the ligand.[11] The nickel-dmbit complexes with several oxidation states were reported and revealed as semiconductor or insulator.[12] Recently, we studied the electrical conductivity and magnetic properties of $(TBA)_{0.29}[Ni(dmbit)_2]$ and $(TBA)_{0.59}[Ni(dmbbip)_2]$ in detail.[14~15] But the monovalent nickel-dmbit and dmbbip complexes were less concerned.

In this paper, we describe the magnetic properties of $(TBA)[Ni(dmbit)_2]$ and $(TBA)[Ni(dmbbip)_2]$ complexes along with the microstructures of the lattices. The magnetic susceptibilities of these complexes are also calculated and explained by fitting with the 2D-Heisenberg antiferromagnetic lattice model. The oxidation state of nickel in monoanionic complexes is confirmed by the results of temperature dependent EPR and magnetic susceptibility, and compared with that of $[Ni(dmit)_2]^{1-}$ complex. Preliminary results of this work have already been reported elsewhere.[16]

Experimental

Synthesis

Organic solvents used in every step were dried over a powder type molecular sieve (4 Å), and deoxygenated by nitrogen bubbling prior to use. All reactions were carried out under nitrogen atmosphere.

1,2,4,5-Tetrakis(isopropylthio)benzene; TPTB. TPTB was prepared by the procedure described in the literature.[17] yield 88%; mp 75 ℃-76 ℃; ^{1}H NMR (300 MHz, $CDCl_3$, TMS) δ [ppm] 7.286 (s, 1H), 3.438 (septet, 2H), 1.317 (d, 12H); ^{13}C NMR (300 MHz, $CDCl_3$, TMS) δ [ppm] 22.928 (8C in CH_3), 37.358 (4C in CH), 132.83 (2C in Bz), 135.88 (4C in Bz); MS (70 eV, 300 ℃ source temperature) m/e 374 (100%, M^+), 332 (23.2%, M^+-$C(CH_3)_2$), 290 (25.3%, M^+-2$C(CH_3)_2$), 248 (39.1%, M^+-3$C(CH_3)_2$), 206 (50.1%, M^+-4$C(CH_3)_2$).

1,3,5,7-Tetrathia-s-indacene-2,6-dithione; TSIT. TSIT was prepared by the procedure described in the literature.[11] yield 95%; mp ~360 ℃ (decomp.); ^{1}H NMR (300 MHz, $CDCl_3$, TMS) δ [ppm] 7.268 (s, 1H); Anal. calc. C (33.08), H (0.70), S (66.23), obs. C (33.20), H (0.75), S (65.85).

5,6-Bis(isopropylthio)benzo[*d*]-1,3-dithiol-2-thione; BPBT. A solution of pyridine (50 mL) with 2.69 mmole of TPTB and 18.0 mmole of sodium metal was stirred at 105 ℃ for 1 hr, and then cooled down to room temperature. It was heated again up to 50 ℃ for 2 hrs after adding 20 mmole of CS_2. De-oxygenated water (10 mL) was rapidly added to the dark-red reaction mixture followd by stirring for 1 hr. The bright-yellow polycrystallines were filtered, washed with de-oxygenated water and minimum amount of cold diethylether and dried *in vacuo*.

yield 95%; mp 143 ℃-144 ℃; ^{1}H NMR (300 MHz, $CDCl_3$, TMS) δ [ppm] 7.353 (s, 1H), 3.469 (septet, 1H), 1.349 (d, 6H); MS (70 eV, 300 ℃ source temperature) m/e 332 (58.7%, M^+), 290 (29.6%, M^+-$C(CH_3)_2$), 248 (100%, M^+-2$C(CH_3)_2$), 204 (20.3%, M^+-2$C(CH_3)_2$-CS); Anal. calc. C (46.95), H (4.85), S

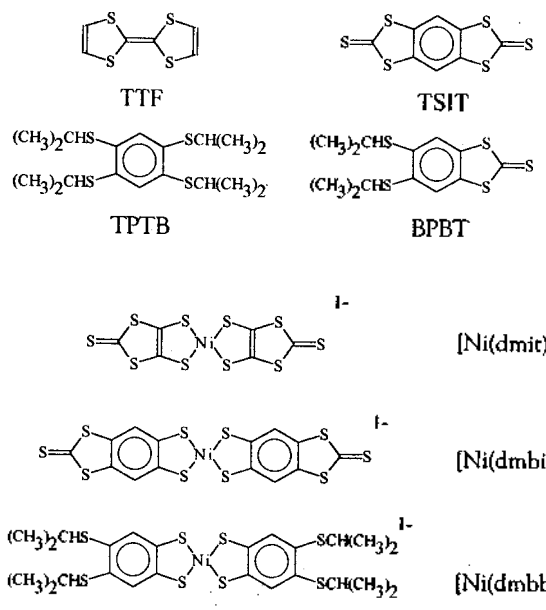

Scheme 1.

(48.20), obs. C (46.90), H (4.82), S (48.21).

Tetra(n-butyl)ammonium bis(5,6-dithio-benzo[*d*]-1, 3-dithiole-2-thione) nickelate(III); (TBA)[Ni(dmbit)$_2$] and Tetra(n-butyl)ammonium bis(1,2-di(isopropyl-thio)benzene-4,5-dithiole) nickelate(III); (TBA)[Ni (dmbbip)$_2$]. The monovalent Ni-dmbit and Ni-dmbbip complexes were prepared and characterized by the procedure described in the literature.[14~15]

Measurements

Chemical analyses, proton NMR, mass spectra and magnetic susceptibility measurements were carried out as described elsewhere.[14] EPR spectra of the polycrystalline complexes were obtained with a BRUKER ER 200D-SRC X-band spectrometer (9.79 GHz) at 300 K and 77 K. The microstructure images of crystals were observed with various magnifications by scanning electron microscope (SEM), JEOL, to confirm the structural characteristics of low-dimensional lattice conformation. Before image generation, samples were coated with gold vapor in the vacuum bell jar for about 1 min.

Results and Discussion

The scanning electron microscopic (SEM) images of [Ni (dmbit)$_2$]^n (n=1, 2) and [Ni(dmbbip)$_2$]$^{1-}$ have been taken and demonstrated in Figure 1, in which they show their structural characteristics: The [Ni(dmbit)$_2$]$^{2-}$ complex shows three-dimensional structure with clear-cut orthorhombic/monoclinic morphologies as shown in Figure 1-A and 1-B. As for the [Ni(dmbit)$_2$]$^{1-}$ complex (Figure 1-C and D) which has been prepared by the iodine oxidation of [Ni(dmbit)$_2$]$^{2-}$, the well-grown two-dimensional layers are regularly stacked forming a layered structure. This morphological distinction could be related to the difference of the oxidation state of anion moiety, [Ni(dmbit)$_2$]$^{n-}$. Also structural anisotropy can be obviously seen in the [Ni(dmbbip)$_2$]$^{1-}$ complex (Figure 1-E and F), where the layers are less closely stacked than

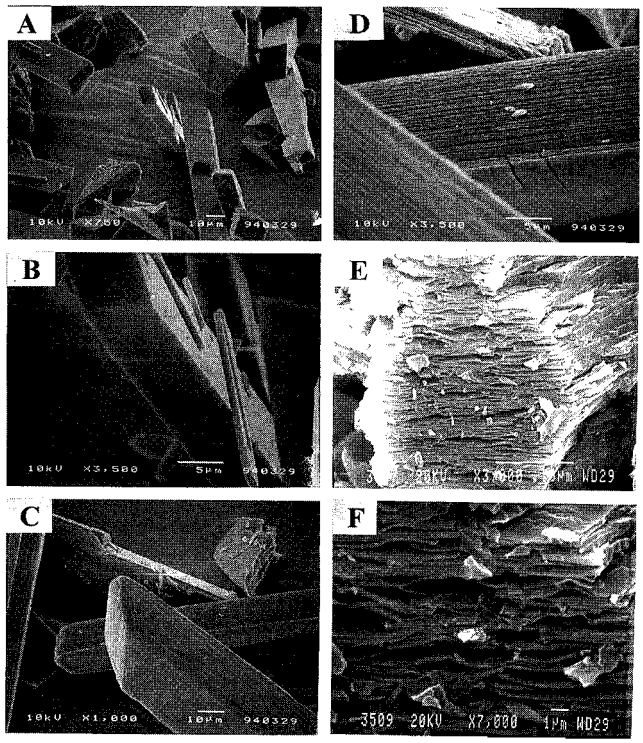

Figure 1. SEM images of (TBA)$_2$[Ni(dmbit)$_2$] (A and B), (TBA) [Ni(dmbit)$_2$] (C and D) and (TBA)[Ni(dmbbip)$_2$] (E and F).

[Ni(dmbit)$_2$]$^{1-}$, probably due to the bulky isopropyl groups on the periphery of dmbbip-ligand. That is, the bulky isopropyl group would prohibit the [Ni(dmbbip)$_2$]$^{1-}$ moieties from close contact so that the loosely-packed structure can be observed. The isopropyl groups on the periphery of dmbbip ligand would also produce an effect on the spin-exchange parameter (J) in the magnetic susceptibility calculations and temperature dependent EPR measurements as will be described below.

The magnetic susceptibilities of polycrystalline [Ni(dmbit)$_2$]$^{1-}$ and [Ni(dmbbip)$_2$]$^{1-}$ complexes measured between 77 K and 300 K have been reported previously,[14] in which they obey Curie-Weiss law, $1/\chi_{m'}=(T-\theta)/Cm$, with the following parameters: Cm=0.38 emu/mol, $\theta=-5.9$ K, $\mu_{eff}=1.74$ B.M for [Ni(dmbit)$_2$]$^{1-}$ and Cm=0.39 emu/mol, $\theta=-3.6$ K, $\mu_{eff}=1.75$ B.M for [Ni(dmbbip)$_2$]$^{1-}$. The negative Weiss constants (θ) represent antiferromagnetic couplings among the nearest-neighboring nickel ions. The effective magnetic moments are very close to the spin-only magnetic moment ($\mu_{s.o}=1.73$ B.M) of low-spin Ni(III) species (d^7, S=1/2).[18] The measured magnetic susceptibilities were in good agreement with the calculated ones (Figure 2 and 3) that can be obtained from the quadratic two-dimensional Heisenberg antiferromagnet model[19~20] expressed by the serial expansion as follow:

$$\frac{Ng^2\mu_B^2}{\chi_c(\Theta)|J|}=3\Theta+\sum_{i=1}^{\infty}\frac{C_i}{\Theta^{i-1}}$$

where the reduced temperature $\Theta=kT/|J|S(S+1)$, J spin-exchange parameter expressed in cm^{-1}, g Lande g-factor, μ_B Bohr magneton and the coefficients $C_i: C_1=4$, $C_2=2.667$, $C_3=1.185$, $C_4=0.149$, $C_5=-0.191$ and $C_6=0.001$ for S=1/2 system. The reliability factor (R) was defined as

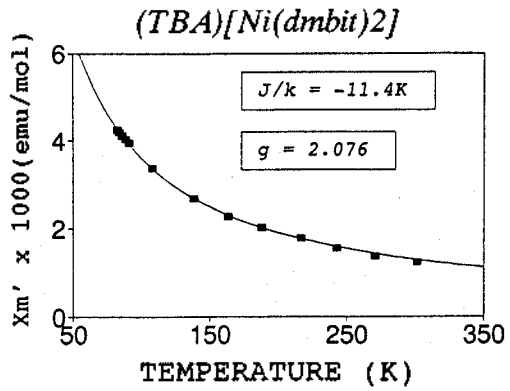

Figure 2. Temperature dependence of magnetic susceptibility (χ_m') for (TBA)[Ni(dmbit)$_2$]. The solid line represents a fit to the calculated series expansion for a two-dimensional Heisenberg-antiferromagnet system.

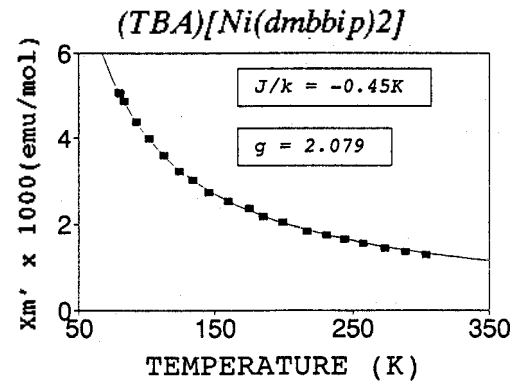

Figure 3. Temperature dependence of magnetic susceptibility (χ_m') for (TBA)[Ni(dmbbip)$_2$]. The solid line represents a fit to the calculated series expansion for a two-dimensional Heisenberg-antiferromagnet system.

$$R=\sum_i (\chi_i^{obs}-\chi_i^{cal})^2/(\chi_i^{obs})^2.$$

The best fit (or the minimized R value) was obtained for [Ni(dmbit)$_2$]$^{1-}$ when $g=2.076$, $J/k=-11.4$ K ($J=-7.9$ cm^{-1}) and $R=9.87\times10^{-5}$. The spin-exchange value is almost same as that of tetraethylammonium salt of [Ni(dddt)$_2$]$^{1-}$ ($J/k=-12.3$ K or $J=-8.5$ cm^{-1}).[8] As for [Ni(dmbbip)$_2$]$^{1-}$, however, smaller J value (-0.31 cm^{-1}) was obtained with the parameters; $g=2.079$ and $R=1.15\times10^{-4}$. This result implies that weaker magnetic interactions are operating among the nearest-neighboring nickel(III) ions than in [Ni(dmbit)$_2$]$^{1-}$ complex. It could also be understood by the morphological defference between [Ni(dmbit)$_2$]$^{1-}$ and [Ni(dmbbip)$_2$]$^{1-}$ complexes as shown in SEM images. The bulky isopropyl group on the periphery of dmbbip ligand could make anion moiety, [Ni(dmbbip)$_2$]$^{1-}$, apart from each other and, therefore, reduce magnetic interactions among the nickel(III) ions.

X-band EPR spectra of polycrystalline [Ni(dmbit)$_2$]$^{1-}$ measured at 300 K and 77 K are demonstrated in Figure 4. It shows apparent axial symmetry at 300 K with anisotropic g-values ($g_{//}=2.158$ and $g_\perp=2.030$) which are compared with those of several monoanionic nickel-bisdithiolenes (Table 1)

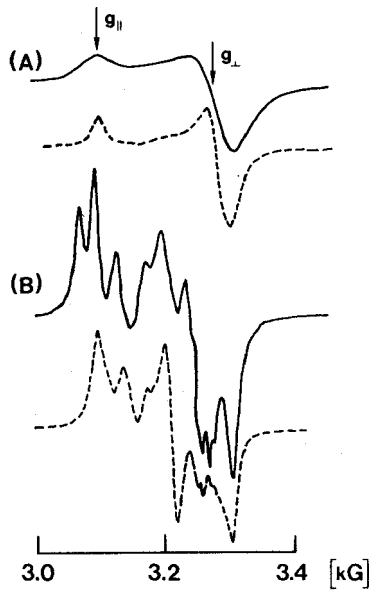

Figure 4. X-band EPR spectra of polycrystalline (A) (TBA)[Ni(dmbit)$_2$] and (B) (TBA)[Ni(dmbbip)$_2$] at 300 K (solid line) and 77 K (broken line), respectively.

Table 1. EPR g-values and magnetic moments of selected monoanionic nickel-1,2-dithiolenes, [NiL$_2$]$^{1-}$

[NiL$_2$]$^{1-}$	g-values				Magnetic moment	Reference
L=	g_1	g_2	g_3	g_{av}	μ (B.M.)	
dmbit	2.158	2.030	2.030	2.074	1.74	this work
dddt	2.119	2.057	2.022	2.066	1.9	8
pddt	2.156	2.070	2.013	2.081	–	10
bdt	2.120	2.109	2.027	2.085	1.83	21
mnt	2.160	2.042	1.988	2.065	–	22

*dddt: 5,6-dihydro-1,4-dithiin-2,3-dithiolate. pddt: 1,3-propanediyldithioethylene-1,2-dithiolate. bdt: o-benzenedithiolate. mnt: maleonitriledithiolate.

containing paramagnetic Ni(III) ion (d^7, S=1/2, $\mu_{s.o}=1.73$ B. M). The [Ni(dmbit)$_2$]$^{2-}$ complex was epr-silent, as expected, possibly due to the diamagnetic Ni(II) ion (d^8, S=0). At 77 K, [Ni(dmbit)$_2$]$^{1-}$ complex exhibits almost the same spectral shape and anisotropic g-values as those at 300 K except for narrow linewidth. This is apparently comparable to the result of [Ni(dmit)$_2$]$^{1-}$ complex[23] which shows isotropic, broad epr signal centered at g=2.04 assigned to the free radical on the dmit-ligand. The axial symmetry in the spectra of Ni-dmbit complex undoubtedly originates from the paramagnetic Ni(III) in anisotropic environment rather than the oxidized dmbit-ligand as in the case of [Ni(dmit)$_2$]$^{1-}$ complex. This difference could be explained by the competition of oxidation between central metal and dithiolene ligand. Dmit-ligand may be more easily oxidized than Ni(II) when [Ni(dmit)$_2$]$^{2-}$ is subjected to be oxidized, and that the free radical is essentially located on the ligand as reported in the literature.[23] On the other hand, dmbit-ligand might be more difficult to

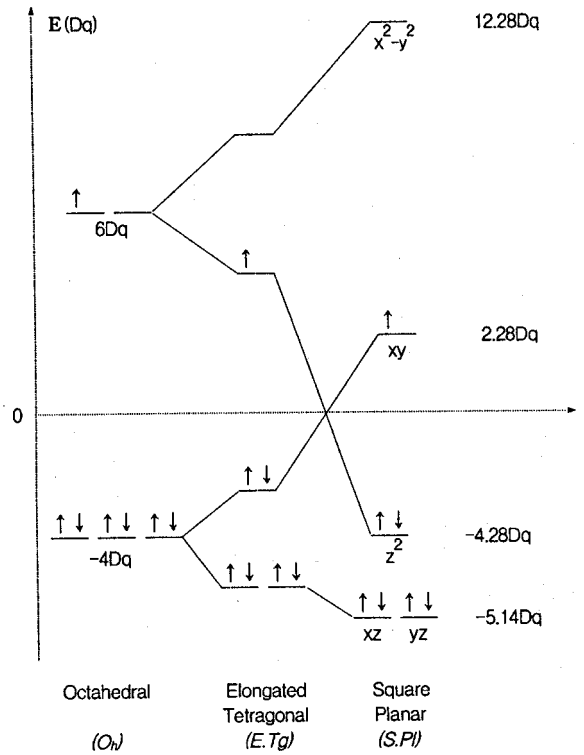

Figure 5. Crystal-field energy diagram of low-spin d^7 transition metal ion in octahedral (O_h), tetragonally elongated (D_{4h}) and square planar (D_{4h}) geometries.

Table 2. EPR g-values of $[Ni^{3+}(dmbit)_2]^{1-}$ at 300 K and 77 K

Temperature	Solid		in MeCN
g-value	300 K	77 K	77 K
$g_{//}$	2.158	2.162	2.082
$g_{\perp}$	2.030	2.038	2.082
g_{av}	2.074	2.080	2.082

be oxidized than Ni(II), because benzene ring is less conjugative with thiocarbonyl group in dmbit-ligand than ethylene moiety is in dmit-ligand[14] and therefore still stabilized with its intrinsic resonance energy. These reactions can be represented as follows:

$$[Ni^{2+}(dmbit)_2]^{2-} \xrightarrow{I_2} [Ni^{3+}(dmbit)_2]^{1-}$$

$$[Ni^{2+}(dmit)_2]^{2-} \xrightarrow{I_2} [Ni^{2+}(dmit)_2]^{1-}$$

As for the low-spin d^7 transition-metal ion in square planar geometry (D_{4h}), crystal-field energy diagram is usually predicted as shown in Figure 5, where the unpaired electron is mainly located in the d_{xy} orbital.[24] The epr g-tensors are also predicted to have the following relationships[25]:

$$g_{xx}=2-\frac{2\lambda}{\Delta E_{xy-xz}} \quad g_{yy}=2-\frac{2\lambda}{\Delta E_{xy-yz}} \quad g_{zz}=2-\frac{8\lambda}{\Delta E_{xy-(x^2-y^2)}}$$

where λ is the spin-orbit coupling constant having negative value for d^7 metal ion, ΔE is the energy separation between the ground and exited states. Although ΔE_{xy-xz} and ΔE_{xy-yz} (7.42 Dq) are smaller than $\Delta E_{xy-(x^2-y^2)}$ (10 Dq) in the square planar geometry where tetragonal elongation is maximized, it is certain that $g_{zz}>g_{xx}$, g_{yy} ($g_{//}>g_{\perp}$) by the factor of 8 in g_{zz}-relation. This is well consistent with the experimental observations (Table 2). Therefore, it is certain that local geometry around the central metal is square planar and the electronic configuration of Ni(III) in $[Ni(dmbit)_2]^{1-}$ complex can be expressed as $(d_{xz}^2 d_{yz}^2 d_{z^2}^2 d_{xy}^1 d_{x^2-y^2}^0)$ within the temperature range measured.

The $[Ni(dmbbip)_2]^{1-}$ complex shows more complicated and significantly different EPR signals at 300 K and 77 K (Fig. 4). Moreover, they are not reproducible even after several hours of equilibrium time. This could be attributted to the irreversible phase transition of $[Ni(dmbbip)_2]^{1-}$ complex mainly promoted by the isopropyl groups on the periphery of dmbbip-ligand, even though the details of phase transition are not able to be explained with these data.

In frozen CH_3CN (77 K), these two nickel(III) complexes identically exhibit only one narrow, isotropic signal ($\Delta H_{pp}\approx$ 100G for $[Ni(dmbit)_2]^{1-}$ and $\Delta H_{pp}\approx$40G for $[Ni(dmbbip)_2]^{1-}$) centered at $g=2.08$ which corresponds to the averaged g-value of solid state $[Ni(dmbit)_2]^{1-}$ at 77 K (Table 5). And they also coincide with the value of Lande g-factor obtained in magnetic susceptibility calculations ($g=2.076$ and 2.079 for $[Ni(dmbit)_2]^{1-}$ and $[Ni(dmbbip)_2]^{1-}$, respectively). It is fairly good agreement between calculated and observed g-values if we consider the fact that the calculated susceptibilities are very sensitive to the small variation of Lande g-factor.

Acknowledgment. This research was supported by Korean Science and Engineering Foundation.

References

1. Brossard, L.; Ribault, M.; Valade, L.; Cassoux, P. *Physica* **1986**, *B143*, 378.
2. Bousseau, M.; Valade, L.; Lagros, J.-P.; Cassoux, P.; Garbauskas, M.; Interrante, L. V. *J. Am. Chem. Soc.* **1986**, *108*, 1908.
3. Ishiguro, T.; Yamaji, K. *Organic Superconductors*; Springer-Verlag: Berlin, 1990.
4. Saito, G.; Kagoshima, S. *The Physics and Chemistry of Organic Superconductor*; Springer-Verlag: Berlin, 1990.
5. Williams, J. M.; Ferraro, J. R.; Thorn, R. J.; Carlson, K. D.; Geiser, Urs; Wang, H. H.; Kini, A. M.; Whangbo, M.-H. *Organic Superconductors*; Prentice Hall: NJ, 1992.
6. For example, $[(CH_3)_2(C_2H_5)_2N][Pd(dmit)_2]_2$: Kobayashi, H.; Bun, K.; Naito, T.; Kato, R.; Kobayashi, A. *Chem. Lett.* **1992**, 1909.
7. Schultz, A. J.; Wang, H. H.; Soderholm, L. C.; Sifter, T. L.; Williams, J. M.; Bechgaard, K.; Whangbo, M.-H. *Inorg. Chem.* **1987**, *26*, 3757.
8. Vance, C. T.; Bereman, R. D.; Bordner, J.; Hatfield, W. E.; Helms, J. H. *Inorg. Chem.* **1985**, *24*, 2905.
9. Kim, H.; Kobayashi, A.; Sasaki, Y.; Kato, R.; Kobayashi, H.; Nakamura, T.; Nogami, T.; Shirota, Y. *Bull. Chem. Soc. Jpn.* **1988**, *61*, 2559.
10. Bereman, R. D.; Lu, H. *Inorg. Chim. Acta* **1993**, *204*, 53.
11. Wolf, P.; M llen, K.; Przybylski, M. *Chimia* **1986**, *40*, 200.

12. Larsen, J.; Bechgaard, K. *J. Org. Chem.* **1987**, *52*, 3285.
13. Le Coustumer, G.; Bennasser, N.; Mollier, Y. *Synth. Metals* **1988**, *B523*, 27.
14. Noh, D.-Y.; Mizuno, M.; Choy, J.-H. *Inorg. Chim. Acta* **1994**, *216*, 147.
15. Noh, D.-Y.; Mizuno, M.; Choy, J.-H. *Synth. Metals* **1993**, *55-57*, 1705.
16. Noh, D.-Y.; Choy, J.-H. *Synth. Metals* **1995**, *70*, 1059.
17. Testaferri, L.; Tiecco, M.; Tingoli, M.; Chianelli, D.; Montanucci, M. *Synthesis* **1983**, 751.
18. Cotton, F. A.; Wilkinson, G. *Advanced Inorganic Chemistry*; 4th. ed., John Wiley & Sons: NY 1980.
19. Rushbrooke, G. S.; Wood, P. J. *Mol. Phys.* **1958**, *1*, 257.
20. Line, M. E. *J. Phys. Chem. Solid* **1970**, *31*, 101.
21. Sandman, D. J.; Allen, G. W.; Acampora, L. A.; Stark, J. C.; Jansen, S.; Jones, M. T.; Ashwell, G. J.; Foxman, B. M. *Inorg. Chem.* **1987**, *26*, 1664.
22. Maki, A. H.; Edelstein, N.; Davison, A.; Holm, R. H. *J. Am. Chem. Soc.* **1964**, *88*, 4876.
23. Sakamoto, Y.; Matsubayashi, G.; Tanaka, T. *Inorg. Chim. Acta* **1986**, *147*, 137.
24. Krishnamurthy, R.; Schaap, W. B. *J. Chem. Educ.* **1969**, *46*, 799.
25. Goodman, B. A.; Raynor, J. B. *Adv. Inorg. Chem. Radiochem.* **1970**, *13*, 135.

Selective Reduction of Carbonyl Compounds with Diisopinocampheylhaloboranes

Jin Soon Cha*, Eun Ju Kim, Oh Oun Kwon, and Jong Mi Kim

Department of Chemistry, Yeungnam University, Kyongsan 712-749, Korea
Received September 27, 1995

Reaction of carbonyl compounds with diisopinocampheylhaloboranes (Ipc_2BX, X=Cl, Br, I) was investigated in detail in order to establish their usefulness as selective reducing agents. The reagents reduced aldehydes and ketones to the corresponding alcohols. The reactivities are in the order of $Ipc_2BCl \gg Ipc_2BBr > Ipc_2BI$. The reagents also reduced α,β-unsaturated aldehydes and ketones to the corresponding allylic alcohols without any detectable 1,4-reduction. Especially, the chloro derivative nicely achieved the selective reduction of aldehyde or ketone groups in the presence of many other functional groups. The most remarkable result of this investigation is that aldehydes and ketones can be selectively reduced in the presence of acid chlorides.

Introduction

Chiral diisopinocampheylchloroborane (Ipc_2BCl) has proven to be extremely efficient for the asymmetric reduction of a wide variety of ketones to obtain chiral alcohols in high enantioselectivities.[1~5] The mechanism of the reduction is explained *via* a cyclic boatlike transition state.[3] The formation of an intermediate alkoxyborane is accompanied by the liberation of α-pinene[3] (Eq. 1). This fascinating reagent attracted

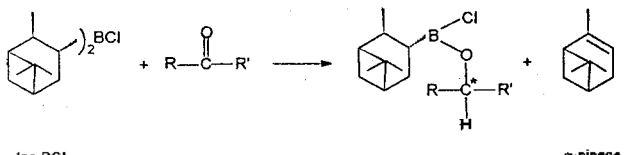

Ipc_2BCl α-pinene

us to investigate its general reducing characteristics in greater detail. Subsequently, we found that the reagent readily reduces α,β-unsaturated aldehydes and ketones to the corresponding allylic alcohols, and permits the selective reduction of aldehyde and ketone groups in the presence of many other functional groups.

Midland and co-workers reported that *B*-alkyl-9-borabicyclo[3.3.1]nonanes (*B*-R-9-BBN) are effective for the reduction of aldehydes, but not for ketones under mild conditions.[6,7] These results indicate that the reduction power of dialkylchloroborane is stronger than that of trialkylborane, particularly in the reduction of carbonyl compounds. The halogen attached to the boron atom seems to exert an additional influence in reduction power.

Accordingly, we decided to extend our investigation to other derivatives, Ipc_2BBr and Ipc_2BI. We prepared a series of diisopinocampheylhaloboranes (Ipc_2BX, X=Cl, Br, I), examined their reactivity toward general organic functional groups, and finally investigated their selectivity in the reduction of carbonyl compounds, in the hope of better understanding the nature of reagents and exploring their role in organic synthesis.

A portion of our results has appeared in the form of preliminary communications.[8,9] We now described in full the results of our study on the reduction characteristics of diisopinocampheylhaloborane.

Results and Discussion

Ipc_2BCl and Ipc_2BBr were prepared from α-pinene by hydroboration followed by treatment with dry hydrogen chloride (HCl) or hydrogen bromide (HBr) in diethyl ether (EE)